Bayesian Estimation of Distance and Surface Normal with a Time-of-Flight Laser Rangefinder

Jochen Lang and Dinesh K. Pai

Laboratory of Computational Intelligence,
Department of Computer Science
University of British Columbia, Vancouver, B.C.
Canada V6T 1Z4.
e-mail: {jlang,pai}@cs.ubc.ca

Abstract

We describe a Bayesian estimation method for measurement of both range and surface orientation using a laser range finder. The method not only provides more accurate estimates of range for dark surfaces that are difficult to measure, but also simultaneously provides estimates of surface normals. This paper describes our efforts for a commercially available sensor, the laser rangefinder Acuity AccuRange 3000 LIR, a widely available device. We detail the Bayesian techniques, sensor calibration, and the processing required.

1. Introduction

Geometric models of pre-existing surfaces are required for many applications including robot navigation on rough terrain, virtual environments, reverse engineering, and architectural walk-throughs. Realistic modeling requires that the models are based on actual measurements, i.e., the model's parameters and their uncertainty are estimated from measurement data and measurement uncertainty. We call these "reality-based" models.

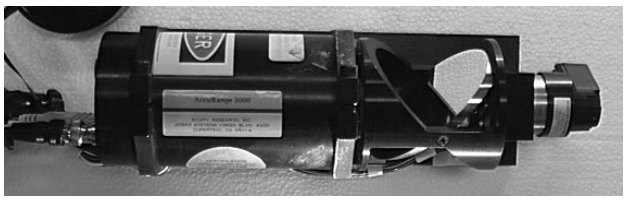

Figure 1. Acuity 3000 LIR

Several technologies are available for measuring range; in this paper we consider a popular type of time-of-flight laser rangefinder (Acuity AccuRange 3000 LIR). This type of scanner is well suited for measuring range over large distances.

However, the raw accuracy of range measurement is relatively poor, particularly for "dark" objects. Range measurement is adversely affected by surface orientation. In addition, many applications of range measurement, such as surface reconstruction, require that surface normals are separately estimated by expensive post-processing of the range data.

In this paper we show how these problems can be addressed simultaneously. By carefully modeling the dependence of range measurements on surface orientation, we can significantly improve range estimates. Somewhat surprisingly, the sensor model shows how to extract useful information about surface orientation as well — effectively allowing a range sensor to be used as a surface orientation sensor.

We consider the Acuity laser rangefinder as a black-box, and improve its performance. The techniques developed here may also be applicable to other complicated measurement devices with unknown internal workings.

The remainder of the paper is organized as follows. Section 2 describes the measurement system used. In Section 3 we outline the estimation method in a simple setting, and introduce Bayesian estimation [2, 5] and sensor modeling. A detailed sensor model is developed in Section 4, and estimation of range and orientation in a realistic setting is described in Section 5. The appendices provide details on preprocessing of rangefinder data and shows some typical results.

2. Measurement system

The range measurement system is part of the UBC Active Measurement Facility (ACME) [8]. This facility is designed to acquire multi-modal data for material and surface properties of small to medium size objects (diameter $\leq 0.5m$). The range measurement setup is is shown in schematic in Figure 2.

The Acuity 3000 LIR is a time-of-flight laser rangefinder; a type of device sometimes also referred to as a LIDAR scanner. The transmitter and receiver are located at the *same* position in the Acuity rangefinder. In the 3000 LIR an infrared laser diode ($780nm$) of $6mW$ is used as the transmitter source. The range finder is fitted with a rotating 45 degree angled mirror producing depth measurements in a plane (see Figure 1). The device is classified as a ANSI class 3b laser product (non-eye-safe). Range measurement is based on the time required by the reflected laser-beam to return to the device. The patented measurement method [3] uses an inverter to switch the laser diode based on the reflected beam, thereby creating an oscillation. The frequency of oscillation depends on the time of travel of the beam. The frequency of oscillation is measured by the device and mapped into a range measurement (see Appendix A for more details).

The beam sweeps out a plane and a measurement consists of the tuple: angular position and range. The angular position of the mirror is sensed by an encoder with 2000 counts per revolution.

3. Method overview

3.1. Bayesian estimation

We develop a Bayesian parameter estimation method to estimate the *true* distance and surface orientation given our measurements for dark surfaces. This produces accurate results despite the very noisy measurements.

The key to using sensor models for estimation is Bayes' theorem. For the laser rangefinder, Bayes' theorem may be expressed as in Equation 1. The background information I contains the knowledge that we dealing with a type of dark material. The term $P(\phi r|I)$ is the bi-variate prior probability distribution for the incidence angle ϕ and distance r given our information. The denominator contains a normalization term $P(D|I)$ which is the measurement probability or prior predictive probability. The sensor model or the sampling probability is $P(D|\phi r I)$. It can be derived from the calibration data, since both the *true* angle of incidence ϕ and the *true* range are known while the measurement data D is recorded. The derivation is detailed below.

$$P(\phi r|DI) = \frac{P(\phi r|I)P(D|\phi r I)}{P(D|I)} \tag{1}$$

Commonly employed least squares routines can be viewed as Bayesian modeling for data errors with a normal distribution.

3.2. Sensor modeling

A sensor model describes the data to be expected given a known entity to be measured. In our situation, we would like to describe the distance measurement process with the rangefinder. In a calibration setup, the distance measurement is compared to a known ground truth. The deviation between the *true* value r and the measured value D is the error e of the sensor in the calibration setup, i.e., $D = r + e$. The error term may be further split into a systematic error e_m and a random error e_σ. Systematic errors are errors which one has knowledge about and plans to model, while random errors one has no suitable model, e.g., their cause is unknown, too complicated or too minor to account for. The systematic error we explore in this paper is the dependence of the distance measurement on the angle of incidence between the laser beam and the surface normal. Please see Figure 4. The dependency of the distance measurement on material properties is also recognized. We model the sensor after the data has been modified by the data processing steps detailed in Appendix B.

3.3. A simple example

In order to outline the process, we will first discuss estimating the distance to the plate and the angle of incidence of the beam on the plate in a simplified configuration that we use for calibration. A more realistic situation is addressed in Section5. In this configuration the plate is upright and the angle of incidence is only dependent on the angular position of the rotation stage and the beam angle α (see Figure 2). Furthermore, the intersection of the plane of the laser beam and plate is at the rotation axis. As a result, for given beam angle α, rotating the plate changes only the angle of incidence but not the point measured with the beam. We assume that we do not know the true distance and the absolute orientation of the plate.

The likelihood, $P(D|r\phi I)$, based on the calibrated sensor model is shown in Figure 3(a). It is a function of r and ϕ given measured data D. Notice that the likelihood has a considerable spread in both range and orientation. This clearly shows the poor accuracy that would be obtained by simply using the raw data. Multiple measurements can now be combined based on the measurement data and the known relative rotation angle between two measurements, using Bayes' theorem. The measurements are always of the same

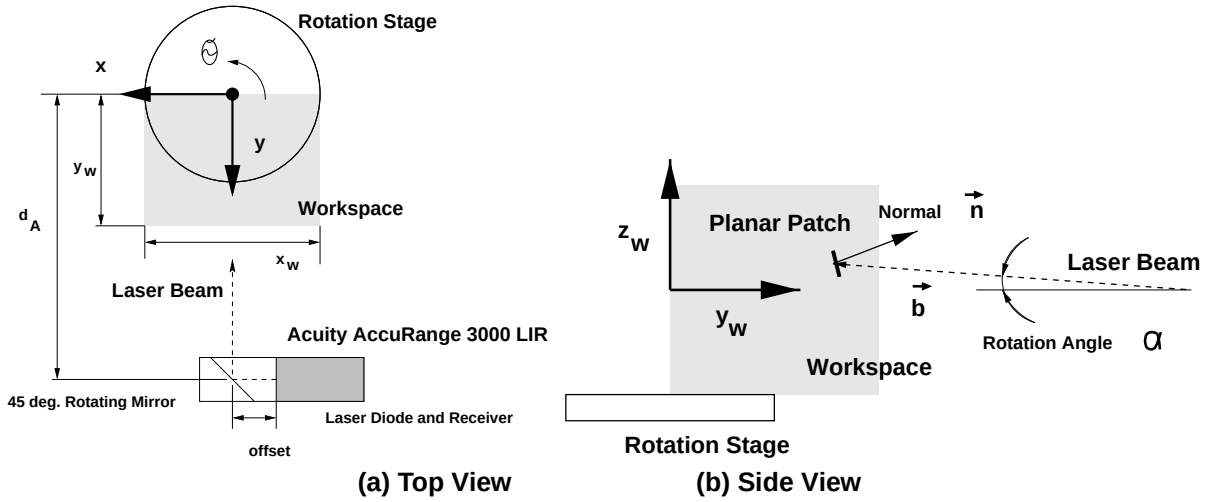

Figure 2. Measurement Setup

point in this simple example, since we use the same beam angle α. The likelihood of the distance and angle of incidence peaks rapidly very close to the *true* solution; the peak is the Maximum Likelihood Estimate of both r and ϕ.

In Section 5, we will extend this simple estimation process to the problem of estimating the position and orientation of a finite but small planar patch not necessarily at the rotation axis.

4. Sensor modeling

In the calibration step, data is gathered in various configurations. The general setup during calibration is shown in Figure 2. A planar metal plate is mounted upright on the rotation stage in the workspace of the rangefinder. The plate surface facing the beam is modified by different colored paper to explore different material properties. The plate is rotated in steps and data is recorded for the intersection of the plane of the laser beam and the plate. Figure 4 shows three examples of calibration data for different colors of paper.

Figure 4 indicates that both the material properties and the angle of incidence influence the measured distance. The error in the data for bright colors is small and detoriates only with very acute angles between surface and beam. However, dark surfaces result in much sparser data and result in large error due to the angle of incidence.

We assume that our range data is normally distributed for a given angle of incidence. This is a very reasonable assumption judging from the calibration data. Keep also in mind that a Gaussian error model is the least informative (or most conservative) error model for a given standard deviation, i.e., if the Gaussian assumption is invalid, we will err on the safe side. The standard deviation of the error is estimated from the sample standard deviation.

Another observation from the calibration data is that noise standard deviation grows with the angle of incidence. To properly account for this variation, we group samples together within narrow bands of angle of incidence. The combined samples in each group and their $\pm 1\sigma_s$ error bars are shown in Figure 5(a).

Bayes' theorem also helps in selecting the model order. We have no further information than the calibration data on the dependence of the distance measurement on the angle of incidence. Therefore, we decide to model the influence with a polynomial of arbitrary order. We use the data to decide which order of polynomial best describes the data. Obviously a higher order polynomial model will always describe data more accurately than a lower order one (the set of higher order models contains the lower order ones).

We use Occam's Razor to decide when over-fitting occurs and employ in accordance with Bayesian probability theory the odds ratio for model comparison (see Equation 2). In the case of competing linear models with equal prior probabilities, the odds ratio can be calculated by Equation 3 [5]. The odds ratio only depends on the difference in the residuals $\Delta\chi = \chi_1 - \chi_2$, the determinant ratio of the covariance matrices dV_2/dV_1 and the difference in the number of model parameters $\Delta n = n_2 - n_1$ times the prior ranges for the linear model coefficient $(\prod_k \Delta A_{k,1})/(\prod_k \Delta A_{k,2})$.

$$O_{i,j} = \frac{P(M_i|I)\ P(D|M_i I)}{P(M_j|I)\ P(D|M_j I)} \quad (2)$$

$$= \exp\frac{\Delta\chi}{2}\sqrt{\frac{dV_2}{dV_1}}(2\pi)^{\frac{\Delta n}{2}}\frac{\prod_k \Delta A_{k,1}}{\prod_k \Delta A_{k,2}} \quad (3)$$

Setting all prior parameter ranges to 1 leads to a ratio of 6.39×10^8:1, 8.86:1, and 0.238:1 for the linear vs. the constant model, the quadratic vs. linear model and the cubic

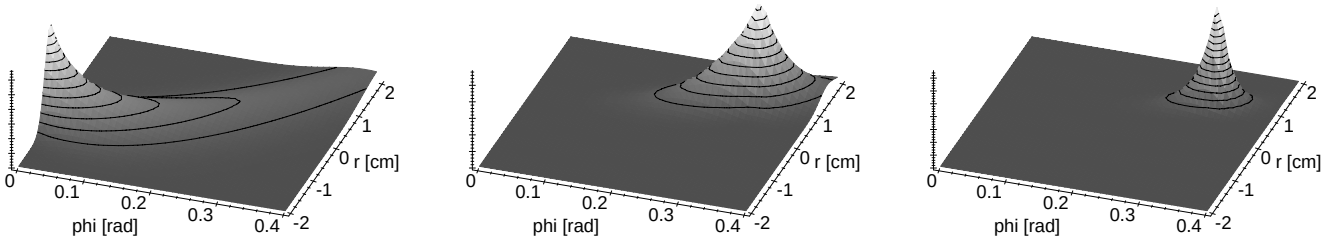

(a) 1 Measurement **(b) 3 Measurements** **(c) 7 Measurements**

Figure 3. Likelihoods, $P(D|r\phi I)$, for simplified experiment (Section 3.3), plotted as function of r relative to D_0 and ϕ.

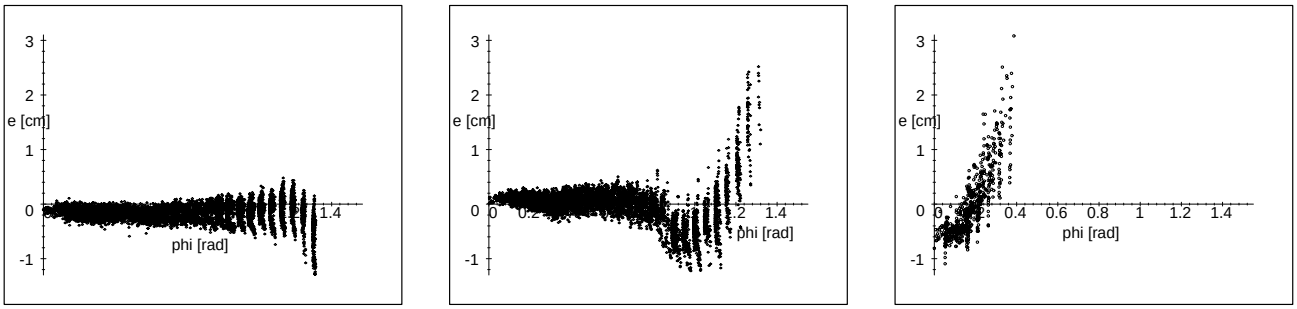

(a) White Paper **(b) Blue Paper** **(c) Black Paper**

Figure 4. Calibration Data. The horizontal axis is labeled with ϕ the angle between incidence laser beam and surface normal. The vertical axis is the error e between *true* distance r and the range reading D.

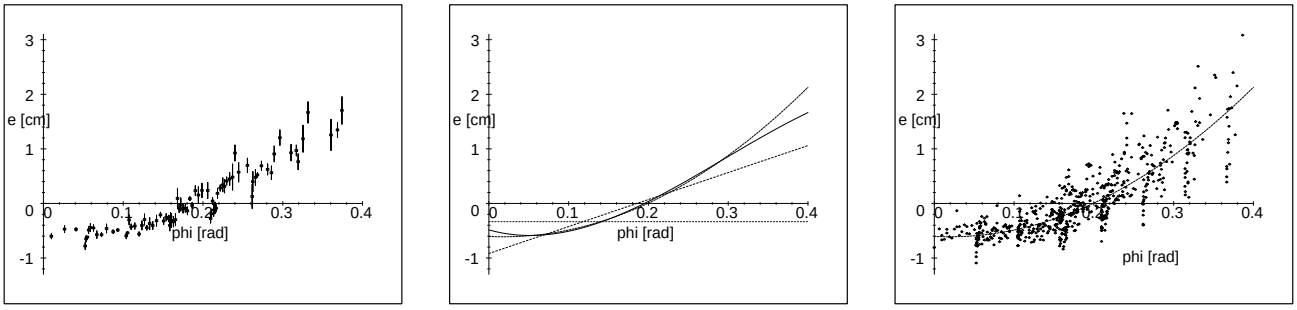

(a) Sample Grouping **(b) Model Comparison** **(c) Final Model**

Figure 5. Sensor Modeling for a Black Target

vs. quadratic model, respectively. Therefore, we decided to employ the quadratic model given in Equation 4, with the coefficients estimated from the calibration data.

$$e_m[cm] = 18.85\ \phi^2 - 0.7102\ \phi - 0.6050 \qquad (4)$$

The systematic error e_m is modeled with Equation 4, however, it remains to model the probabilistic error term e_σ. The probabilistic error term is modeled with a normal distribution. As noted previously, the probabilistic error is also dependent on the angle of incidence. This is obvious from the plot of the residual of the quadratic model fit vs. the angle of incidence in Figure 6(a). We employ a strategy very similar to that used for the systematic error model. First, the variance of the residual is calculated for narrow ranges of incidence angles. The standard derivation of this variance is expected to decrease with the square root of the number of samples used for the estimation. The resulting variance estimation and their $\pm 1\sigma_s$ is shown in Figure 6(b).

The model comparison yields odds ratios of 5.85:1 and 0.520:1 for the linear over the constant and the quadratic vs. linear model, respectively. Therefore, the linear model in Equation 5 is chosen. The overall model in Equation 6 follows.

$$\sigma[cm] = 1.353\ \phi + 0.06082 \qquad (5)$$

$$P(D|r\phi I) = \frac{1}{\sqrt{2\pi}\sigma} \exp \frac{-(D-(e_m+r))^2}{2\sigma^2} \qquad (6)$$

This completes the sensor modeling task. We will now explore the use of the model to arrive at better estimates of distance (and angle of incidence) given measurements taken with the sensor.

5. Planar patch estimation

The sensor returns a one-dimensional distance measurement. However, the sensor model developed in Section 4 is two-dimensional (see Equation 6).

One possibility is to simply choose to marginalize over the additional dimension — the angle of incidence ϕ. This requires solving the integral $P(r|DI) = \int d\phi\ P(r\phi|DI)$. The resulting distance estimates recognizing the angular dependency should be an improvement on a simple averaging of measurements. Averaging distance measurements can only reduce the probabilistic error to zero in the limit but would not be capable of reducing the systematic error due to the dependency on the angle of incidence.

Rather than treating the dependency of the distance measurement on the angle of incidence as a nuisance, we exploit this dependency to estimate both the distance and the angle of incidence.

In order to extend the estimation process to a surface of arbitrary orientation and position anywhere in the rangefinder's workspace, a surface model is required. This requirement stems from two facts: on the one hand we would like to fully utilize the bi-variate sensor model to learn about the distance r to a surface and the angle of incidence ϕ at the same time; and on the other hand, we need a method to combine measurements if the change in angle of incidence between measurements is unknown (unlike the situation in Section 3.3). For simplicity, we choose a planar patch as a surface model rather than a more elaborate or more extended model.

A planar patch in the workspace of the laser can be parameterized as in Equation 7. This parameterization excludes planes parallel to the $y-z$ plane and $x-y$ plane; these however cannot be imaged by the rangefinder in the first place. Given a planar patch and the knowledge of the position and the orientation of the rangefinder, the angle of incidence between the beam $\vec{b}$ and the surface normal $\vec{n}$ is calculated as in Equation 8. The range is found with Equation 9 (see coordinate frame assignment in Figure 2). The patch is rigidly attached to the rotation stage since it is assumed to be on an object placed on the stage. The rotation stage can rotate the object by a rotation angle θ and the stage itself can be moved along the x-axis by t_x and y-axis by t_y through two additional translation stages. The equation of the rotated patch in the original coordinate system is given by Equation 10.

$$0 = a\ x + b\ y + c\ z + d \quad \text{with } b = 1 \qquad (7)$$

$$\phi = \arccos\left(\frac{-b\cos\alpha + c\sin\alpha}{\sqrt{a^2+b^2+c^2}}\right) \qquad (8)$$

$$r = \frac{b\ d_A + d}{b\cos\alpha - c\sin\alpha} \qquad (9)$$

$$\begin{aligned} a' &= a\ \cos\theta - b\ \sin\theta \\ b' &= a\ \sin\theta - b\ \cos\theta \\ c' &= c \\ d' &= -at_y\ \sin\theta + at_x\ \cos\theta \\ &\quad -bt_y\ \cos\theta + bt_x\ \sin\theta + d \end{aligned} \qquad (10)$$

The next step in the process of the planar patch estimation is the application of Bayes' theorem to this case. Equation 11 sketches the derivation based on the independence of the measurements and the relation $P(abcd|r\phi)$ being deterministic. The prior $P(r\phi|I)$ is set to be uniform over the range of distances and angles of incidence we expect to see. The sensor model $P(D_i|r\phi I)$ has been derived in Section 4. Equations 7 - 10 provide an indexing function into the r - ϕ space of the measurement data.

$$P(abcd|D_0 \ldots D_k I) = \int_r \int_\phi P(abcdr\phi|D_0 \ldots D_k I),$$

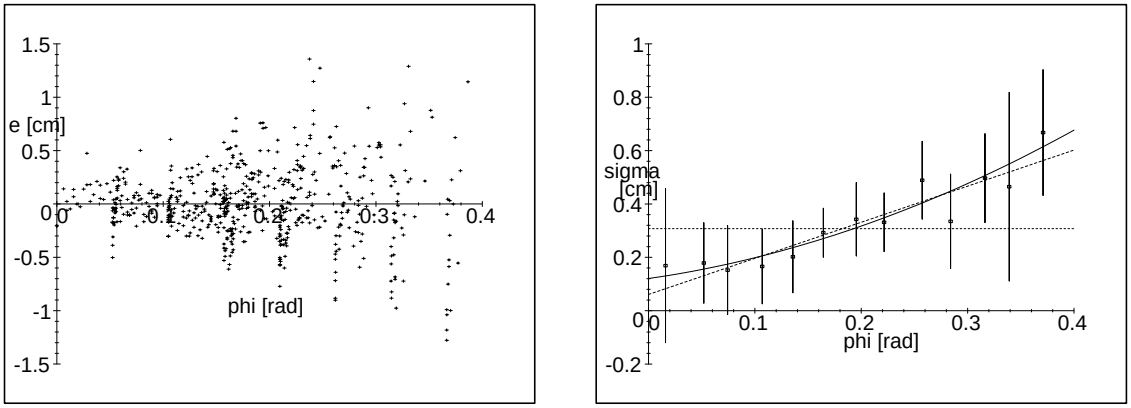

(a) Residual of Systematic Error Fit (Quadratic) **(b) Variance Model**

Figure 6. Dependency of Probabilistic Sensor Error on Angle of Incidence

$$= \int_r \int_\phi P(abcd|r\phi D_0 \dots D_k I) P(r\phi|D_0 \dots D_k I),$$
$$= P(r(a,b,c,d)\phi(a,b,c)|D_0 \dots D_k I),$$

since r and ϕ are deterministic functions of a, b, c, d. Therefore,

$$P(abcd|D_0 \dots D_k I) \propto$$
$$P(r\phi|I) P(D_0|r\phi I) P(D_1|r\phi I) \dots P(D_k|r\phi I). \quad (11)$$

In order to clarify the procedure, we will repeat the simple demonstration case of Section 3.3 but with the above developed machinery. It is sufficient to set $a = 0$ *a priori* corresponding to upright planes and to notice that this results in a 1:1 mapping between the r - ϕ space and the space c - d at $a = 0$ of the planar patch. The most likely patch corresponds then to the peak in the likelihood in r - ϕ space. The result of our discrete evaluation yields $c = 0.295$ and $d = -1.0$ for a patch on the calibration plate at $\alpha = 0$ from the same measurements as in Section 3.3.

6. Results

We will now report two applications of our planar patch estimation method. One application involves black metal plates at varying position and orientation, for which the results are listed in Table 1. The other application are planar patches along the cylindrical wall of a dark painted beverage can. The results for the can are easily judged by inspection and shown in Figure 7.

In this first application the plates are mounted away from the rotation-axis at different angles. The translation and rotation stages are employed to ensure that the measured point is always within a small patch. The minimum size of the patch is determined from the error in an initial distance estimate, as well as by the location of the patch relative to the rotation axis. The distance to the plate is erroneous at first, since it is initially estimated from only one orientation. The three-dimensional space of patches is difficult to visualize, therefore, we only list the most likely patch found by our estimation process in Table 1. Observe the well estimated normal of the planar patch.

The application of our model to the dark painted beverage can requires modeling the sensor for the material of the can. We follow the same procedure as outlined in Section 4. The calibration data was gathered by viewing a vertical line on the cylindrical can from various angles (assuming the can along the vertical scanline is straight). The parameters for this model (Equation 6) are the systematic error in Equation 12 and the probabilistic error in Equation 13.

$$e_m[cm] = 10.53\,\phi^2 + 1.387\,\phi + 1.588 \quad (12)$$
$$\sigma[cm] = 1.159\,\phi + 0.1452 \quad (13)$$

We estimate a planar patch along the cylindrical wall of the can. This plane is an estimate of the tangent plane to the can since we only use data along the same scanline. The approximation is based on three depth images of the can which are at $0.08727 rad(5\,\mathrm{deg})$ relative to each other. The images were taken by translating the can in steps parallel to the scanning plane of the rangefinder. The depth images were mapped into a common coordinate frame and the resulting point cloud is shown in Figure 7(a). The point cloud shows a very distinct parabolic rather than circular shape of the can when viewed from the top.

Application of the planar patch estimation procedure of Section 5 provides the parameters of the planar patch (still represented by the implicit model $0 = ax + y + cz + d$). The position and the normal of the central point of the patch a-

Actual		Estimated		Samples		
Normal	Distance $[cm]$	Normal	Distance $[cm]$	No.	θ-steps $[rad]$	α-range $[rad]$
$\begin{bmatrix} 0.0 \\ 1.0 \\ -0.105 \end{bmatrix}$	~ 50	$\begin{bmatrix} -0.0093 \\ 1.0 \\ -0.1023 \end{bmatrix}$	49.50	132	$-0.2618, -0.1745,$ $-0.08727, 0, 0.08727,$ $0.1745, 0.2618$	$-0.03142 \ldots 0.03142$
$\begin{bmatrix} 0.0 \\ 1.0 \\ 0.131 \end{bmatrix}$	~ 50	$\begin{bmatrix} -0.0092 \\ 1.0 \\ 0.1100 \end{bmatrix}$	51.64	132	$-0.2618, 0, 0.2618$	$-0.05969 \ldots 0.05969$
$\begin{bmatrix} 0.0 \\ 1.0 \\ 0.2618 \end{bmatrix}$	~ 50	$\begin{bmatrix} -0.0284 \\ 1.0 \\ 0.2180 \end{bmatrix}$	52.04	87	$-0.1745, -0.08727,$ $0, 0.08727, 0.1745$	$-0.03142 \ldots 0.03142$

Table 1. Summary of Results

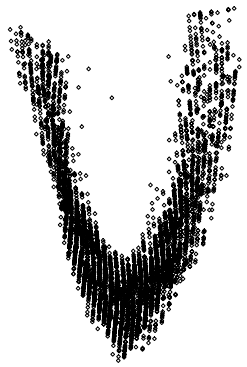

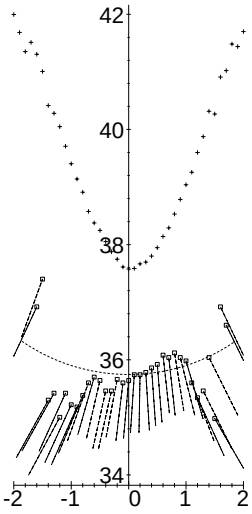

(a) Point Cloud viewed from Top

(b) Comparison between "True" Surface (Dotted Line), Simple Averaging (Cross) and Our Patch Estimation Method (Box and Solid Line)

Figure 7. Planar Surface Patch Reconstruction for Dark Beverage Can

long the scanline is shown in Figure 7(b). The position and normal are computed from the most likely patch for each scan line respectively (the likelihood is three-dimensional in the parameters a, c and d of the implicit model). For comparison the *true* shape of the can as well as the result of *naive* averaging is shown. The application of our sensor model to planar patch estimation leads to a drastic improvement over *naive* averaging and is fairly close to the real shape of the can.

7. Conclusion

We have shown that the application of Bayesian probability theory to measurements with a typical laser rangefinder improves the accuracy of range measurements, and it is even possible to exploit the systematic measurement errors to extract orientation information. Probability theory provides the tools to deal with low intensity measurements due to material properties of the imaged surface and the very subtle systematic dependence of the noise on the surface orientation. The process employs a planar surface model which has to be a suitable model for all measurements of the same patch. This patch can be very small. The method could also be extended to a variety of surface models. We aim to incorporate the described techniques in the UBC Active Measurement Facility (ACME) [8], our multi-modal active object modeling facility.

In future work, we plan to develop faster methods for finding the MAP (maximum a posteriori) estimate for a surface patch, and to design an active sensing algorithm which exploits our estimation method. Our current method relies on prior sensor calibration for material; in the future we hope to better understand the nature of this dependence on material type.

Acknowledgments

The financial support of the Federal Networks of Centres of Excellence IRIS project and NSERC Canada is gratefully acknowledged. We thank Dr. R.J. Woodham for his valuable input to parts of this work.

References

[1] M.D. Adams and P.J. Probert. The integration of phase and intensity data from amcw light detection sensors for reliable ranging. *IJRR*, 15(5), 1996.

[2] G.L. Bretthorst. *Bayesian spectrum analysis and parameter estimation*. Springer-Verlag, New York, 1988.

[3] R.R. Clark. Scanning rangefinder with range to frequency conversion. US Patent 5,309,212, May, 3rd 1994.

[4] D.C. Cramer and L.M. Peterson. Lasar radar in robotics. *Proc. of the IEEE*, 84(2):299–320, 1996.

[5] P.C. Gregory. *Measurement theory and bayesian data analysis*. Lecture notes in physics 509, 1997. UBC, Vancouver, Canada, to appear.

[6] M. Hebert and E. Krotkov. 3d measurements from imaging laser radars: How good are they? *Image and Vision Computing*, 10(3):170–178, 1992.

[7] J. Kostamovaara, K. Määttä, M. Kosjinnen, and Myllylä R. Pulsed laser radars with high modulation-frequency in industrial applications. In *Laser Radar VI*, volume V. 1633, pages 114–127. SPIE, 1995.

[8] D.K. Pai, J. Lang, J.E. Lloyd, and R.J. Woodham. ACME, a telerobotic active measurement facility. In *International Symposium on Experimental Robotics*, volume 6, Sydney, Australia, March 1999.

[9] M. Wellfare, L. Love, K. McCarthy, and L. Prestwood. Ladar image synthesis with comprehensive laser model. In *Laser Radar Technology and Applications*, volume V. 2748, pages 208–219. SPIE, 1996.

A. Acuity 3000 LIR operation

In the design of time-of-flight laser rangefinders several inherent difficulties need to be addressed [7, 9] (most of these problems are similar to modulated continuous-wave rangefinders [6, 4]). The times to be measured are extremely short (travel time at the speed of light); therefore, the electronic circuits measuring the time suffer from thermal drift. The Acuity addresses this problem somewhat by measuring frequency based on several periods instead of the direct travel time of the beam. It also simultaneously measures the temperature with the time-of-flight. The reflection of the beam at an object depends on the object's surface, i.e., on the angle of incidence between the beam and the surface, as well as the reflectance properties of the surface. The intensity of the reflected beam at the receiver somewhat characterizes the reflectance properties of the surface. The intensity is also measured simultaneously with range by the Acuity (like most similar devices - often classified as imaging laser rangefinders). The Acuity employs a calibration look-up table to map a measurement triplet of frequency, intensity and temperature into a range reading.

B. Data processing

The image processing steps added to the Acuity blackbox aim to address some major errors observed in the data: outliers (often due to mixed pixels [1]: reflection of the finite size laser beam from multiple surfaces at different depth in one measurement), missed absolute orientation pulse, thermal drift (which is still present after Acuity's look-up calibration) and white noise.

Figure 8(a) shows a typical result of a scan indoors. Notice the mixed pixels in form of single measurement points

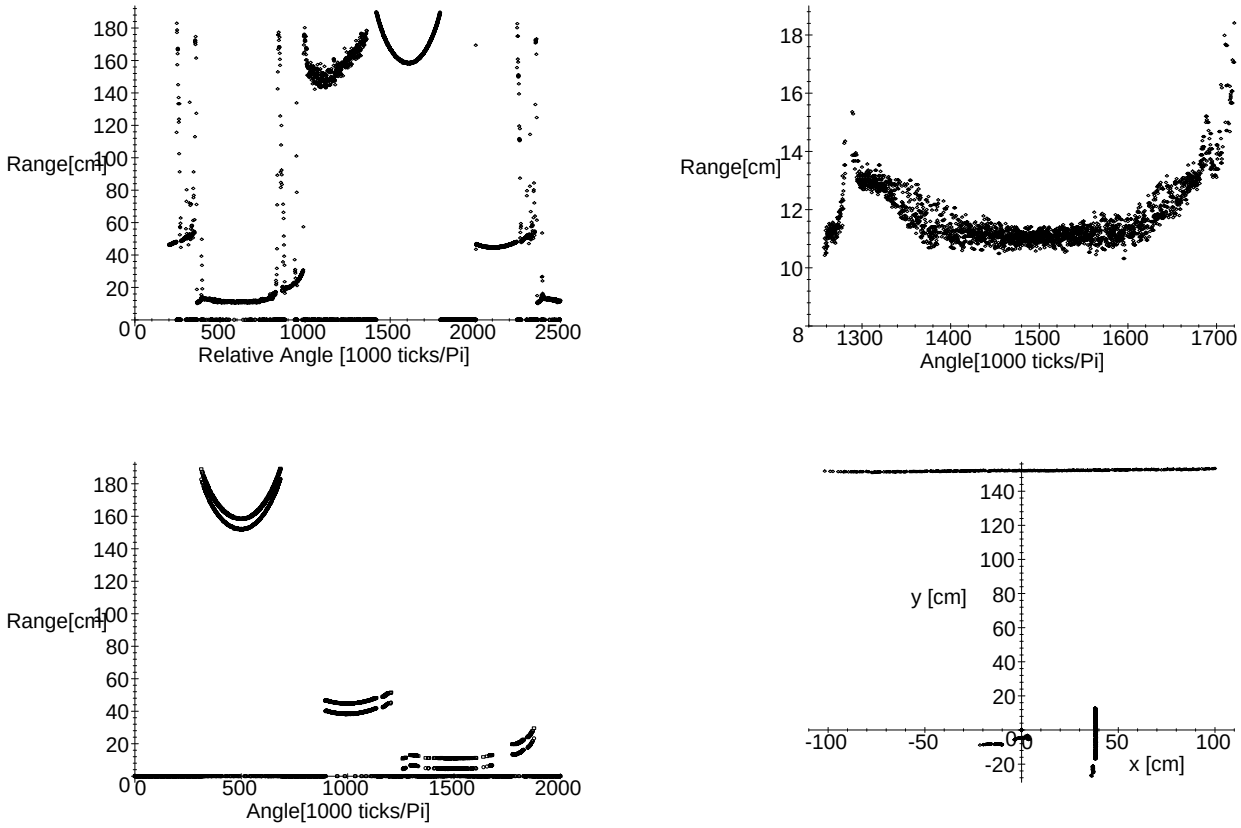

Top Row: (a) Scan before Image Processing (b) Scan Detail: Mounting Plate
Bottom Row: (c) Filtered and Offset Compensated Scan (d) Scan after Image Processing

Figure 8. Image Processing Steps for a Typical Indoor Scene

between continuous segments in the scan. Also notice the influence of surface material increasing the width of some segments with respect to others. The scan is in units of range in cm over device angular ticks. The range distance contains an offset value for the beam length due to the distance between transmitter and rotating mirror, and between rotating mirror and receiver.

The detection of gross outliers is simple given two assumptions: (i) all scanned reflecting surfaces are continuous for at least two consecutive range readings and (ii) the receiver only sees a reflection for surfaces for which the incidence angle of the beam is greater than a breakdown angle.

We modeled the result of the thermal drift as a constant range offset. The offset due to thermal drift and the distance between mirror transceiver can be corrected based on a static mounting plate in the laser plane of view (see Figure 8(b)).

A median filter is applied to repeated scans. The median filter is followed by averaging of measurements within a given band of the median (see Figure 8(b) for the mounting plate before filtering and Figure 8(c) for the scan after filtering and offset correction). Assuming the noise of the measurements has a zero mean, this filter makes it reasonable that the noise of the average can be modeled with a Gaussian distribution (Central Limit Theorem).

Missing of the absolute orientation can be corrected by registering several scans together. The registration finds the orientation of a scan with unknown absolute orientation relative to a scan with known absolute orientation. However, it was found that repeating scans until an absolute orientation is successfully read is often faster. Therefore, the current implementation attempts to find the absolute orientation of a scan in three steps: it keeps scanning until success or for a maximum fixed (8) number of times, failing this it tries to register the section corresponding to the mounting plate of the laser, and finally, if this fails it registers the whole scan by correlation (see Figure 8(d)).